The Astrophysical Journal Letters, 853:L17 (6pp), 2018 January 20 https://doi.org/10.3847/2041-8213/aaa756

Quasi-periodic Behavior of Mini-disks in Binary Black Holes Approaching Merger

Dennis B. Bowen[1], Vassilios Mewes[1], Manuela Campanelli[1], Scott C. Noble[2,3,6], Julian H. Krolik[4], and Miguel Zilhão[5]
[1] Center for Computational Relativity and Gravitation, Rochester Institute of Technology, Rochester, NY 14623, USA; dbbsma@rit.edu
[2] Department of Physics and Engineering Physics, The University of Tulsa, Tulsa, OK 74104, USA
[3] Goddard Space Flight Center, Greenbelt, MD 20771, USA
[4] Department of Physics and Astronomy, Johns Hopkins University, Baltimore, MD 21218, USA
[5] CENTRA, Departamento de Física, Instituto Superior Técnico, Universidade de Lisboa, 1049 Lisboa, Portugal
Received 2017 December 14; revised 2018 January 9; accepted 2018 January 12; published 2018 January 24

Abstract

We present the first magnetohydrodynamic simulation in which a circumbinary disk around a relativistic binary black hole feeds mass to individual accretion disks ("mini-disks") around each black hole. Mass flow through the accretion streams linking the circumbinary disk to the mini-disks is modulated quasi-periodically by the streams' interaction with a nonlinear $m = 1$ density feature, or "lump," at the inner edge of the circumbinary disk: the stream supplying each mini-disk comes into phase with the lump at a frequency 0.74 times the binary orbital frequency. Because the binary is relativistic, the tidal truncation radii of the mini-disks are not much larger than their innermost stable circular orbits; consequently, the mini-disks' inflow times are shorter than the conventional estimate and are comparable to the stream modulation period. As a result, the mini-disks are always in inflow disequilibrium, with their masses and spiral density wave structures responding to the stream's quasi-periodic modulation. The fluctuations in each mini-disk's mass are so large that as much as 75% of the total mini-disk mass can be contained within a single mini-disk. Such quasi-periodic modulation of the mini-disk structure may introduce distinctive time-dependent features in the binary's electromagnetic emission.

Key words: accretion, accretion disks – black hole physics – magnetohydrodynamics (MHD)

1. Introduction

Supermassive binary black holes (SMBBHs) are expected to form following galaxy mergers (see Khan et al. 2016 and Kelley et al. 2017 for recent work). When copious gas is available, SMBBHs may be luminous electromagnetically as a result of accretion. Newtonian simulations including the black holes (BHs) in the computational domain have demonstrated that the accreting material from the circumbinary disk forms individual mini-disks around each BH (Roedig et al. 2012; Farris et al. 2014, 2015a, 2015b; Muñoz & Lai 2016; Tang et al. 2017, 2018). The spectra of these systems may exhibit distinctive features, both in the infrared/optical range and in hard X-rays (Roedig et al. 2014). It is also important to predict the character of their electromagnetic emission later in the binary's history, as it approaches merger, both for its intrinsic interest and because the behavior of gas in this period creates the conditions upon which the merger acts. Unfortunately, simulations of matter flowing from a circumbinary disk to a BBH system in the relativistic regime have been unable to form any such mini-disks (Bode et al. 2010, 2012; Palenzuela et al. 2010; Farris et al. 2011, 2012; Giacomazzo et al. 2012; Gold et al. 2014). However, if mini-disks are placed in such a system, hydrodynamic simulations have found that they remain stable down to a binary separation $a \lesssim 20M$[7] (Bowen et al. 2017).

In this Letter, we present the first-ever general relativistic magnetohydrodynamic (MHD) simulation in which matter is accreted from a circumbinary disk into the domain of a relativistic BBH with mini-disks around the BHs. We observe a dynamic coupling between the accretion streams linking the circumbinary disk to the mini-disks and an $m = 1$ modulation of the gas density at the inner edge of the circumbinary disk, a "lump." Each BH comes into phase with the lump at a rate equal to the beat frequency between the lump's orbital frequency and the binary orbital frequency ($\Omega_{\rm bin}$), $\approx 0.74\Omega_{\rm bin}$; while in phase, a BH's accretion stream carries more material than the other BH's stream. The stronger stream then alternates from one BH to the other.

This lump-driven asymmetric accretion has been observed in previous simulations (Noble et al. 2012; Shi et al. 2012; D'Orazio et al. 2013, 2016; Farris et al. 2014, 2015a, 2015b), but when the binary separation is relativistic it leads to more dramatic consequences. Newtonian studies with two mini-disks (Farris et al. 2014, 2015a, 2015b) produced nearly identical mini-disks for equal-mass binaries. By contrast, in these relativistic binaries the relatively modest distance from a mini-disk's tidal truncation radius to its innermost stable circular orbit (ISCO) implies an inflow time comparable to the stream alternation period; as a result, the mini-disks' internal structures, accretion rates, and masses vary strongly on the alternation timescale, keeping the mini-disks in a permanent state of inflow disequilibrium.

2. Simulation Details

2.1. General Relativistic Magnetohydrodynamics

The aim of our simulation is to investigate the dynamics of individual mini-disks due to their interaction with the accretion from the inner edge of the circumbinary disk when the binary's orbit is relativistic. We approximate the spacetime of the binary by asymptotically matching BH perturbation theory to post-Newtonian (PN) theory; this description satisfies the Einstein Field Equations well in the regime of this study (for full details see Noble et al. 2012; Mundim et al. 2014; Ireland et al. 2016;

[6] NASA Postdoctoral Program Senior Fellow.
[7] We adopt geometrized units with $G = c = 1$ where $r_g \equiv GM/c^2$ and M is the total mass of the binary.

Bowen et al. 2017). We evolve the equations of general relativistic MHD on this background spacetime in flux-conservative form using the HARM3D code (see Noble et al. 2009, 2012; Bowen et al. 2017), neglecting the self-gravity of the gas because the gas mass is negligible in comparison to the SMBBH's mass for astrophysically relevant systems.

The gas's thermodynamics is governed by an adiabatic equation of state and local cooling. We cool toward the system's initial local entropy via the prescription of Noble et al. (2012). Following Bowen et al. (2017), the cooling time is set differently in each of four distinct regions; one for the circumbinary region ($r > 1.5a$), one for each mini-disk ($r_i < 0.45a$), and one for the cavity between the mini-disk and circumbinary regions. Here, r and r_i denote the distance to the center of mass and individual ith BH, respectively. The cooling time is taken to be the local, equatorial Keplerian orbital period of the fluid in the circumbinary and mini-disk regions. Everywhere else, the cooling time is taken as that for $r = 1.5a$. For full details on the calculations of these cooling times see Bowen et al. (2017).

2.2. Grid and Boundary Conditions

We perform our simulation in a dynamic, double fish-eye (warped) spherical PN harmonic coordinate system whose origin lies at the center-of-mass (Zilhão & Noble 2014). This system concentrates cells in the immediate vicinity of the BHs in order to resolve the mini-disks, while smoothly transitioning to spherical coordinates in the circumbinary disk. See Zilhão & Noble (2014) and Bowen et al. (2017) for further insight into the grid structure employed.

We excise a sphere of radius $r = 2M$ around the origin at the center of mass because the warped coordinates are topologically spherical. Although this cutout removes material sloshing between the two mini-disks (Bowen et al. 2017), an excision region this large enlarges the time step sufficiently for this simulation to run within our available resources. We impose outflow boundary conditions on the "radial" x^1 boundaries, requiring that the radial component of the 4-velocity u^r be either zero or oriented out of the domain on the boundary. The outer boundary is located at $13a_0$, where a_0 is the initial binary separation. We apply reflective axisymmetric boundary conditions at the "polar angle" x^2 boundaries and periodic boundary conditions at the "azimuthal" x^3 boundaries.

We use $600 \times 160 \times 640$ ($x^1 \times x^2 \times x^3$) cells. The equatorial plane cell counts were chosen to follow Bowen et al. (2017). The poloidal cell count does not fully meet the standard of 32 cells per scale height in the outer portions of the mini-disks on the side farthest from the center of mass, but it allows the simulation to be accessible with our available resources; in the circumbinary disk, we use a poloidal grid identical to that of Noble et al. (2012), who demonstrated that it provides good quality resolution.

2.3. Initial Data

We initialize our simulation using two separate regions, one for the domain of the mini-disks ($r < a_0$) and another for the circumbinary data. The initial state of the circumbinary disk is the equilibrated state of RunSE in Noble et al. (2012) at $t = 50{,}000M$. This time was selected to ensure that the disk had sufficiently equilibrated in terms of MHD turbulence and azimuthally averaged surface density, and had also begun to break axisymmetry near its inner edge. The circumbinary data were obtained from a simulation that employed a different coordinate basis and grid discretization from the one used for our present simulation, so we needed to perform a tri-linear interpolation onto our grid. However, this interpolation step introduces violations to the magnetic field divergence constraint.

We remove the divergence from, or "clean," our solution by employing a projection method (Brackbill & Barnes 1980; Tóth 2000) until ≈99% of the domain reaches a target of

$$\nabla \cdot \boldsymbol{B} \leqslant 10^{-3} b_\lambda b^\lambda / dx^i_{\rm min}\,, \tag{1}$$

where b_λ is the magnetic 4-vector and $dx^i_{\rm min}$ is the smallest cell dimension anywhere in the grid.

For the mini-disk region ($r < a_0$), we initialize nearly hydrostationary torii around each BH, neglecting the presence of the binary companion (Bowen et al. 2017). For this study, we extended the method to include an initial seed magnetic field and the vertical structure of the disks. In the local Boyer–Lindquist frame of each BH we set the time, radial, and polar angle components of the vector potential to zero, but set

$$A_{\phi_{\rm BL}} = \max\left(\bar{\rho} - \frac{1}{4}\rho_{\rm max}, 0\right), \tag{2}$$

where $\bar{\rho}$ is the average density of a cell and its neighbors and $\rho_{\rm max}$ is the maximum density of the mini-disk. A_μ is then transformed into and interpolated onto the warped grid. Finally, we calculate the magnetic field and normalize it to produce the desired initial plasma β. The full details of the mini-disk initialization are described in Bowen et al. (2017).

We select the mini-disk initial parameters to be $r_{\rm in} = 3.1M$, $r_{\rm pmax} = 4.6M$, $\beta = 100$, $H/r_{\rm pmax} = 0.09$ (H is the vertical scale height), and initial entropy $S_0 \equiv P/\rho^{5/3} = 0.01$. These values were chosen so that in their initial state the mini-disks were wholly outside the ISCO and had structural properties, but not necessarily inflow rates, similar to those of the initial circumbinary disk.

3. Results

Our simulation starts with an initial binary separation $a_0 = 20M$ (defined in the PN harmonic gauge), a distance chosen so that low-order (1PN) effects are $\sim O(0.1)$ and binary inspiral due to gravitational radiation is noticeable, but small, over the duration of a simulation. As observed in Bowen et al. (2017), there is a brief initial transient in which the mini-disks expand because tidal forces were neglected in their construction. After about a binary orbital period, the mini-disks become tidally truncated at $r_t \simeq 0.3a$ and begin to accrete onto their individual BHs. Meanwhile, the circumbinary disk delivers mass to the mini-disks through a pair of accretion streams that forms almost immediately.

As can be readily gleaned from Figure 1, the two accretion streams are not symmetric, and the contrast in their mass content grows with time. The more massive stream always has its origin in the lump at the inner edge of the circumbinary disk. Due to this asymmetry, the streams preferentially deposit material onto one of the mini-disks at any given time, despite the BH's equal masses. We examine this effect in greater detail in the next subsection.

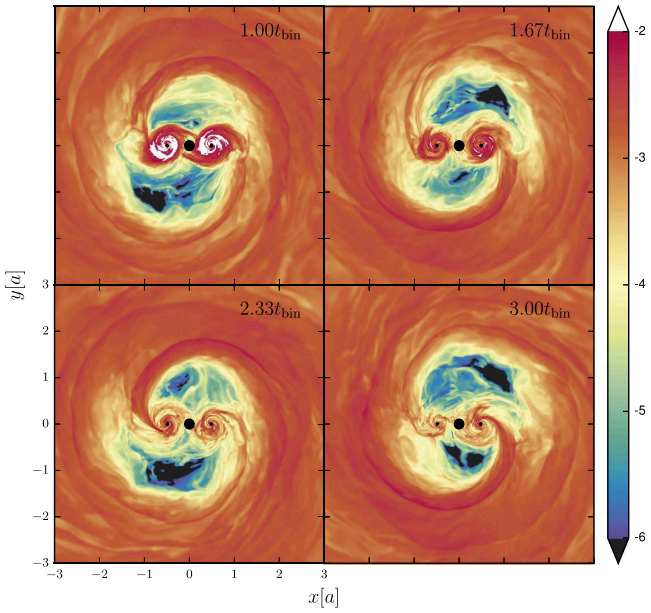

Figure 1. Logarithmic density contours in the equatorial plane of the binary. Simulation time in units of the binary's orbital period is denoted in the top right of each frame. Each BH is represented by a black circle and the larger black circle at the coordinate origin marks the central cutout of the simulation.

3.1. Asymmetric Accretion into the Central Cavity

The circumbinary disk is turbulent, but supports a lump at $r \approx 2.4a$. The peak surface density of the lump is nearly $4\times$ the mean surface density of the circumbinary and extends over ≈1–2 radians in azimuth. Within $r \approx 2a$, there is a low-density cavity across which the streams travel toward the mini-disks. These features are shown in Figure 1, which portrays, in a frame corotating with the binary, the gas density in the equatorial plane at intervals of $\approx(2/3)t_{\rm bin}$, where $t_{\rm bin} = 2\pi/\Omega_{\rm bin}$. In this frame, the accretion streams are almost fixed in position, although their mass content fluctuates.

The times of the four images in Figure 1 were chosen so as to highlight a striking effect of the stream asymmetry. From one to the next, the BH receiving the most matter changes. It is BH2 (on the left) in the first frame, BH1 (on the right) in the next, back to BH2 in the third, and BH1 in the fourth. This alternation has its origin in the stationarity of the $m = 2$ accretion stream pattern in the corotating frame. Relative to this stationary pattern, the lump moves backward, so that it feeds first one stream and then the other.

Previous MHD simulations have shown that the lump orbits at the local Keplerian frequency, $\Omega_{\rm lump} = \Omega_K(r = 2.4a) = 0.26\Omega_{\rm bin}$ (Noble et al. 2012; Shi et al. 2012). Therefore, one or the other of the BHs comes into phase with the lump at a frequency $2(\Omega_{\rm bin} - \Omega_{\rm lump}) = 1.48\Omega_{\rm bin}$. Each individual BH does so at precisely half this frequency, $0.74\Omega_{\rm bin}$.

We illustrate this switch in preferential accretion more quantitatively in Figure 2 by plotting the radially and vertically averaged azimuthal mass-flux of the accretion streams in a frame corotating with the binary. This component of the flux provides a good approximation to the mass accretion rate because in this frame the dominant flow of the streams is in the azimuthal direction. We find a clear, quasi-periodic oscillation in which the azimuthal location of the flux switches from near one BH to near the other and back again. The diagonal wedges

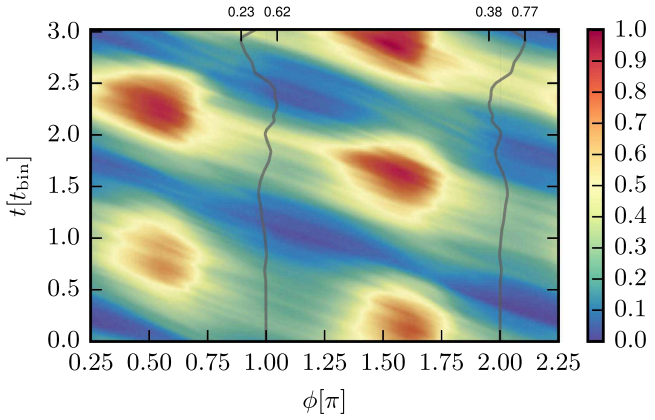

Figure 2. (Color contours) Time and azimuthal dependence of the radially and poloidally averaged azimuthal mass-flux (ρv^ϕ), normalized to the peak value in the simulation, in the frame corotating with the binary. v^ϕ denotes the azimuthal component of the 3-velocity. Radial and poloidal averaging is taken for $r \in (1.5a, 2.0a)$ and $\theta \in (0.4\pi, 0.6\pi)$, respectively. Azimuthal angle is shifted by 0.25π so that the stream accreting onto Disk 1 ($\phi = 2\pi$) and Disk 2 ($\phi = \pi$) are always to the left of the disk for clarity. (Vertical lines) The BH locations are marked by straight lines. Semi-transparent lines denote the fraction of combined mini-disk mass as a function of time within each disk, where shifts to the left or right correspond to less than and more than half the mass, respectively. Individual labels at the top provide the minimum and maximum value for scale.

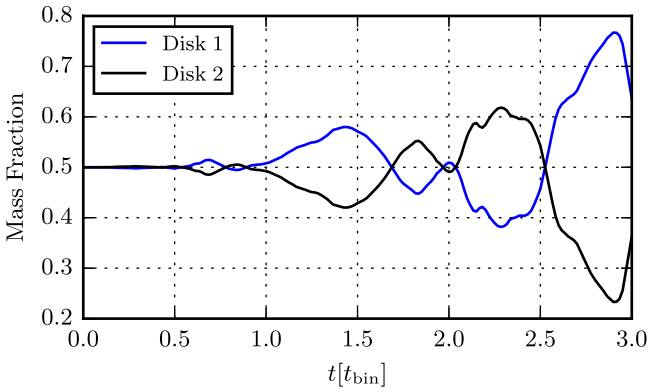

Figure 3. Time dependence of the mass contained within each mini-disk ($r_i \leqslant 0.4a_0$) normalized to the combined mass of both mini-disks. Disk 1 and Disk 2 denote the mini-disks around BH1 and BH2, respectively.

are a result of the time delay as the stream moves from the inner edge of the circumbinary to its target mini-disk. The period of these oscillations is consistent with the beat frequency just estimated, $\approx(2/3)t_{\rm bin}$.

In addition to a quasi-periodic oscillation from one mini-disk to the other, Figure 2 demonstrates that the magnitude of the mass-flux in the dominant accretion stream increases with time. Conversely, the low flux state between lump-driven accretion events lack such growth. Finally, we note that the lump has been shown to grow secularly over many binary orbits (Noble et al. 2012; Shi et al. 2012). Such growth could enhance the observed effect.

3.2. Depletion and Refilling Cycle of Relativistic Mini-disks

The preferential accretion described in Section 3.1 leads to two mini-disks whose internal structures differ and never approach steady-state. A simple global measure of these facts is the time dependence of the mini-disks' masses. In Figure 3, we plot the fraction of total mini-disk mass contained within each

disk. The mini-disks' mass fractions oscillate, while their contrast continually grows; shortly before the end of the simulation the mini-disk around BH1 contains over three times the mass of the other mini-disk.

The first two panels of Figure 1 are at $t/t_{\rm bin} = 1.0$, 1.67, times when, according to Figure 3, the two disk masses are nearly equal; the other two panels are at $t/t_{\rm bin} = 2.33$, 3.0, when the disk masses are near their peak contrasts. The more massive stream initially feeds the less massive mini-disk while the other mini-disk drains. After some time, as seen in the latter two snapshots, the more massive stream's mini-disk becomes the larger one. In addition, at the later times, the denser stream extends further into the mini-disk it feeds. In fact, after $t \approx 2t_{\rm bin}$, the stream deposits its material onto the mini-disk at radii well within the tidal truncation radius, sometimes reaching almost to the ISCO. Further evidence for the connection between preferential disk feeding and mass contrast can be drawn from comparing Figures 2 and 3. The times of greatest mini-disk mass contrast coincide with the times of greatest stream mass-flux contrast.

If the inflow time within a mini-disk were well predicted by the classical α model (as assumed in Farris et al. 2014, 2015a, 2015b), it would be

$$t_{\rm inflow} \sim [\alpha(H/R)^2\Omega_t]^{-1} \sim 80(\alpha/0.1)^{-1}[(H/r)/0.1]^{-2}t_{\rm bin}, \quad (3)$$

where Ω_t is the local orbital velocity at the outer edge of the mini-disk. Because the mini-disks in our simulation change in mass on much shorter timescales, $\sim 0.5t_{\rm bin}$, it is clear that other mechanisms must be at work. We discuss what they might be in Section 4.

3.3. Spiral Density Waves

As Figure 1 makes plain, strong spiral shocks are a persistent feature of these mini-disks. Unlike those seen in the purely hydrodynamic simulations of Ryan & MacFadyen (2017), they are highly irregular and non-steady. This contrast is in keeping with the Newtonian results of Ju et al. (2016), who demonstrated that MHD turbulence can have this effect on spiral shocks in binary systems. Spiral waves can be excited near Lindblad resonances in mini-disks by a binary companion's tidal gravity (Goldreich & Tremaine 1979; Papaloizou & Lin 1984; Savonije et al. 1994). They are of special interest because once they become nonlinear and steepen into shocks, they can exert stresses on the fluid (Papaloizou & Lin 1995; Goodman & Rafikov 2001; Heinemann & Papaloizou 2012; Rafikov 2016); where they travel slower than the orbital velocity of the fluid, these stresses transport angular momentum outward, facilitating accretion (Ju et al. 2016; Mewes et al. 2016).

In Newtonian gravity (Savonije et al. 1994; Makita et al. 2000; Ju et al. 2016) and in relativistic simulations using a Newtonian perturber (Ryan & MacFadyen 2017), the spiral patterns have pure $m = 2$ character because the dominant azimuthal Fourier component of the Newtonian perturbing potential is $m = 2$ (Savonije et al. 1994). However, the perturbing potential in our relativistic binary spacetime has a significant $m = 1$ contribution (Bowen et al. 2017).

To quantify the non-axisymmetric mode strength, we compute the normalized azimuthal Fourier amplitudes of the density (Zurek & Benz 1986; Heemskerk et al. 1992). Figure 4 shows the resulting mode strengths for each mini-disk and the total mode strength. As found by Bowen et al. (2017), the dominant Fourier mode is $m = 1$. However, unlike Bowen et al. (2017), who found significant contributions from only $m = 1$ and $m = 2$, we observe lesser, but noticeable, $m = 3$ and $m = 4$ contributions. Moreover, the amplitude of all disk modes grow in time. Interestingly, the total mode strength in each mini-disk is greatest when its mass is greatest.

In the classical picture, spiral waves are excited only by tidal gravity. However, spiral waves in accreting mini-disks may be incited by pressure waves arising from the impact of accretion streams. Accretion streams also alter the spiral wave character by raising the local gas temperature when they strike the mini-disks: where the ratio of gas temperature to virial temperature is higher, spiral waves are less tightly wound and can propagate inward to smaller radii (Savonije et al. 1994; Ju et al. 2016).

4. Discussion and Conclusions

4.1. Disk-mass Oscillations in Relativistic Binaries

Analytic accounts of gas flow in binaries with near-unity mass ratios initially assumed mini-disks would not exist at all (Pringle 1991; Milosavljević & Phinney 2005); more recent analytic work assumed that that they would have near-equal masses and maintain a state of inflow equilibrium (Roedig et al. 2014). Some simulations (Farris et al. 2014, 2015a, 2015b) have found results consistent with these expectations. In sharp contrast, in our equal mass-ratio simulation, the mini-disks' masses are in general quite different from one another and are far from inflow equilibrium at all times.

The reason why our results are so different stems largely from the relativistically close separation of the binary we treat. The outer edge of the mini-disk in an equal-mass binary, even in the relativistic regime, is $r_t \approx 0.3a$ (Bowen et al. 2017). For a binary separation of $20M$ and a non-spinning BH, $r_t \approx 2.4r_{\rm ISCO}$ ($r_{\rm ISCO} = 2.5M$ in PN harmonic coordinates); this close to the ISCO, the inflow rate is no longer well described by the classic estimate $\sim\alpha(H/R)^2\Omega$. In fact, explicit simulation of relativistic accretion onto single black holes has shown that in this regime inflow is considerably faster: at $r/r_{\rm ISCO} \simeq 2$, Krolik et al. (2005) found an inflow time of only $\simeq 7$ local orbital periods for a disk in which $H/R \simeq 0.15$ (similar to our mini-disks). Assuming Keplerian orbits, this inflow time corresponds to $\approx 1.5t_{\rm bin}$ for our simulation. Part of this inflow acceleration is due to the significant radial pressure gradient near the ISCO. Another part is due to the fact that the local specific angular momentum in this region is not much larger than that at the ISCO. As a result, less stress is required to move inward (this is the flip-side of the well-known torque reduction factor; Page & Thorne 1974). If the stress nonetheless remains large, as it can be when due to MHD turbulence, inflow can be accelerated. In a binary whose mini-disks are relatively hot, as our mini-disks are, spiral shocks can augment angular momentum transport and make inflow even swifter.

In a simple model of the stream alternation, the accretion rate onto a mini-disk might be described as a mean rate plus a sinusoidal modulation of fractional amplitude ϵ and frequency $\omega_{\rm mod}$. In such a case, the fractional amplitude of the oscillations in mini-disk mass would be

$$f_{\rm mass} = \frac{\epsilon}{[1 + (\omega_{\rm mod}t_{\rm inflow})^2]^{1/2}}. \quad (4)$$

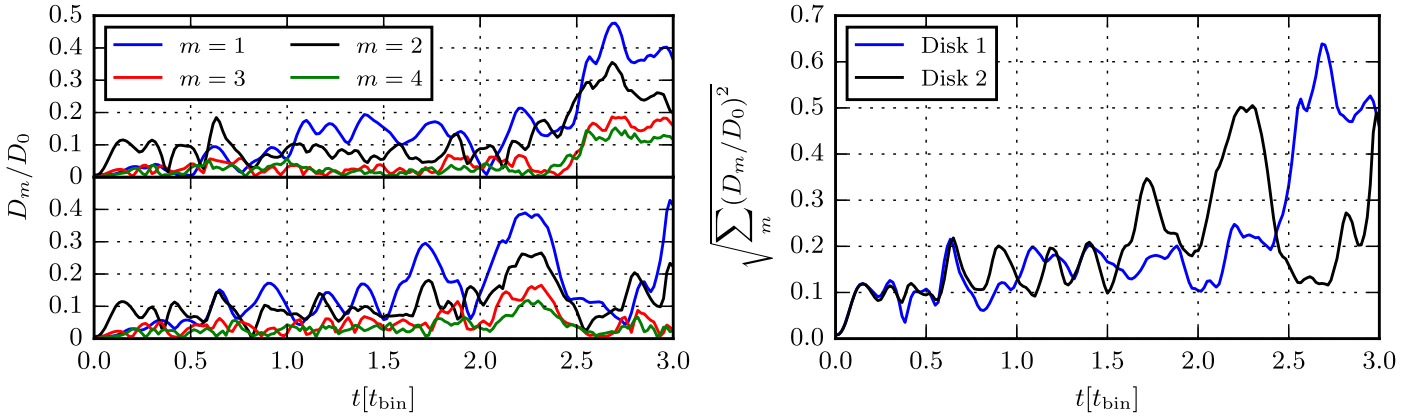

Figure 4. (Left) Time dependence of the $m = 1$ to $m = 4$ modes of the density in (top) Disk 1 and (bottom) Disk 2. (Right) Time dependence of the total mode strength, up to the $m = 4$, within each mini-disk.

In earlier work (Farris et al. 2014, 2015a, 2015b), $\omega_{\rm mod}\, t_{\rm inflow}$ was $\gg 1$, making $f_{\rm mass} \ll \epsilon$, because the binary separation was taken to be large enough that classical inflow rate estimates applied. In our case, however, $\omega_{\rm mod} = 0.74\Omega_{\rm bin}$ and $t_{\rm inflow} = 1.5t_{\rm bin}$, leading to $f_{\rm mass} \simeq \epsilon/7$. However, the actual situation departs from this simple model in two ways: the total accretion rate onto the binary increases over time, and fluctuations in the structure of the mini-disks can lead to corresponding fluctuations in $t_{\rm inflow}$. In particular, as already mentioned, the depletion of the mini-disks, combined with the increased mass-flow in the streams, permits the streams to reach well within the nominal truncation radius. Thus, especially in the second half of the simulation, the matter actually joins the mini-disk at a radius where $t_{\rm inflow}$ is considerably shorter than $\approx 1.5t_{\rm bin}$, leading to much larger excursions in mass than predicted by the simple modulation model.

Although our simulations demonstrate that very large amplitude modulation of the mini-disk masses and accretion rates can happen, it would be premature to claim that it is general for SMBBHs with $a = 20M$. If the BHs spin rapidly, the ISCO would move inward, increasing $t_{\rm inflow}$. Both magnetic stress and spiral shocks are more effective when H/R is relatively large, and mini-disks with lower accretion rates may be cooler than those simulated here.

In addition, the asymmetry in stream mass-fluxes depends on the amplitude of the lump, but its dependence on system parameters has not yet been well explored. It may decrease in magnitude as mass-ratio q drops from ~ 1 to ~ 0.1 (D'Orazio et al. 2013, 2016). In binaries with smaller q, accretion into the central cavity preferentially targets the secondary. This effect would diminish the alternating contrast between the accretion rates onto the two mini-disks and instead create a quasi-periodic modulation of the accretion rate onto the secondary's mini-disk. Nonetheless, if the separation is small enough that the secondary's mini-disk extends to only a few ISCO radii, the inflow time could still be short enough for the secondary mini-disk's mass to follow the modulated accretion rate.

A further potential complication has to do with "decoupling" dynamics, the events occurring when the inflow time in the *circumbinary* disk becomes longer than the orbital evolution time (Milosavljević & Phinney 2005). For the parameters of this simulation, Noble et al. (2012) showed that decoupling as it is generally envisioned never happens, so that accretion continues all the way through to merger. However, it remains possible that for circumbinary disks with smaller H/R, the binary separation at which "decoupling" occurs may be considerably larger than the $\sim 20M$ at which it occurred for their (and our) simulation. In such a case, the binary can evolve to a state in which its orbital frequency is much greater than the orbital frequency at the inner edge of the circumbinary disk, likely washing out accretion modulation due to the lump. Finally, the ratio $(r_t/r_{\rm ISCO})$ will continue to shrink as the binary inspirals toward merger. This shrinkage may further enhance the depletion/refilling cycle up until the point at which distinct mini-disks disappear.

4.2. Further Implications

Just as their structure is quite different from the usual picture of disks in inflow equilibrium, the radiation produced by mini-disks in the state we have found should also be quite different from the predictions of such steady-state models. Moreover, their intrinsically transient character makes application of the traditional α model for local dissipation suspect. Instead, estimates of the emitted light require direct use of local heating rates due to MHD turbulent dissipation and shocks. A first discussion of the electromagnetic emission from the mini-disks we simulated is presented in a companion publication (S. d'Ascoli et al. 2018, in preparation).

We conclude by mentioning that in our previous treatment of relativistic mini-disks in 2d hydrodynamics, we found substantial "sloshing," gas exchange between the mini-disks through the L1 region (Bowen et al. 2017; such exchange can be seen in the first frame of Figure 1). In our present simulation, however, at times later than shown in that panel, the large central cutout intercepted most such streams, removing their mass from the system. In the absence of such a cutout, we expect that the sloshing will follow the mini-disk asymmetry, with more material entering the sloshing region from the more massive mini-disk than the less massive mini-disk. This mechanism, given a significant mini-disk mass asymmetry, might diminish the mass disparity between the mini-disks, but the degree to which it does will depend on the detailed mass distribution and internal flow pattern of the more massive mini-disk. Using the PATCHWORK framework (Shiokawa et al. 2017), which will eliminate the cutout at the center of mass, we intend in the near future to determine what effect sloshing may have on mini-disk mass variation. With that additional information, it will also be possible to explore the

consequences for photons radiated by the entire mini-disk system, including the sloshing material.

We thank Mark J. Avara for a careful reading of this manuscript and for helpful discussions and suggestions. D.B. would also like to thank Brennan Ireland for helpful discussions. We would like to thank the anonymous referee for the careful reading of this manuscript and for the helpful comments and questions raised. D.B., M.C., V.M., and M.Z. received support from NSF grants AST-1028087, AST-1516150, PHY-1305730, PHY-1707946, OAC-1550436, and OAC-1516125. S.C.N. was supported by AST-1028087, AST-1515982, and OAC-1515969, and by an appointment to the NASA Postdoctoral Program at the Goddard Space Flight Center administrated by USRA through a contract with NASA. J.H.K. was partially supported by NSF grants AST-1516299, PHYS-1707826, and OAC-1516247. V.M. also acknowledges partial support from AYA2015-66899-C2-1-P. M.Z. acknowledges support through the FCT (Portugal) IF programme, IF/00729/2015.

Computational resources were provided by the Blue Waters sustained-petascale computing NSF projects OAC-0832606, OAC-1238993, OAC-1516247 and OAC-1515969, OAC-0725070. Blue Waters is a joint effort of the University of Illinois at Urbana-Champaign and its National Center for Supercomputing Applications. Additional resources were provided by XSEDE allocation TG-PHY060027N and by the BlueSky Cluster at Rochester Institute of Technology. The BlueSky cluster was supported by NSF grants AST-1028087, PHY-0722703, and PHY-1229173.

ORCID iDs

Dennis B. Bowen https://orcid.org/0000-0002-7447-1142
Vassilios Mewes https://orcid.org/0000-0001-5869-8542
Scott C. Noble https://orcid.org/0000-0003-3547-8306
Julian H. Krolik https://orcid.org/0000-0002-2995-7717

References

Bode, T., Bogdanović, T., Haas, R., et al. 2012, ApJ, 744, 45
Bode, T., Haas, R., Bogdanović, T., Laguna, P., & Shoemaker, D. 2010, ApJ, 715, 1117
Bowen, D. B., Campanelli, M., Krolik, J. H., Mewes, V., & Noble, S. C. 2017, ApJ, 838, 42
Brackbill, J. U., & Barnes, D. C. 1980, JCoPh, 35, 426
D'Orazio, D. J., Haiman, Z., Duffell, P., MacFadyen, A., & Farris, B. 2016, MNRAS, 459, 2379
D'Orazio, D. J., Haiman, Z., & MacFadyen, A. 2013, MNRAS, 436, 2997
Farris, B. D., Duffell, P., MacFadyen, A. I., & Haiman, Z. 2014, ApJ, 783, 134
Farris, B. D., Duffell, P., MacFadyen, A. I., & Haiman, Z. 2015a, MNRAS, 447, L80
Farris, B. D., Duffell, P., MacFadyen, A. I., & Haiman, Z. 2015b, MNRAS, 446, L36
Farris, B. D., Gold, R., Paschalidis, V., Etienne, Z. B., & Shapiro, S. L. 2012, PhRvL, 109, 221102
Farris, B. D., Liu, Y. T., & Shapiro, S. L. 2011, PhRvD, 84, 024024
Giacomazzo, B., Baker, J. G., Miller, M. C., Reynolds, C. S., & van Meter, J. R 2012, ApJL, 752, L15
Gold, R., Paschalidis, V., Etienne, Z. B., Shapiro, S. L., & Pfeiffer, H. P. 2014, PhRvD, 89, 064060
Goldreich, P., & Tremaine, S. 1979, ApJ, 233, 857
Goodman, J., & Rafikov, R. R. 2001, ApJ, 552, 793
Heemskerk, M. H. M., Papaloizou, J. C., & Savonije, G. J. 1992, A&A, 260, 161
Heinemann, T., & Papaloizou, J. C. B. 2012, MNRAS, 419, 1085
Ireland, B., Mundim, B. C., Nakano, H., & Campanelli, M. 2016, PhRvD, 93, 104057
Ju, W., Stone, J. M., & Zhu, Z. 2016, ApJ, 823, 81
Kelley, L. Z., Blecha, L., & Hernquist, L. 2017, MNRAS, 464, 3131
Khan, F. M., Fiacconi, D., Mayer, L., Berczik, P., & Just, A. 2016, ApJ, 828, 73
Krolik, J. H., Hawley, J. F., & Hirose, S. 2005, ApJ, 622, 1008
Makita, M., Miyawaki, K., & Matsuda, T. 2000, MNRAS, 316, 906
Mewes, V., Galeazzi, F., Font, J. A., Montero, P. J., & Stergioulas, N. 2016, MNRAS, 461, 2480
Milosavljević, M., & Phinney, E. S. 2005, ApJL, 622, L93
Mundim, B. C., Nakano, H., Yunes, N., et al. 2014, PhRvD, 89, 084008
Muñoz, D. J., & Lai, D. 2016, ApJ, 827, 43
Noble, S. C., Krolik, J. H., & Hawley, J. F. 2009, ApJ, 692, 411
Noble, S. C., Mundim, B. C., Nakano, H., et al. 2012, ApJ, 755, 51
Page, D. N., & Thorne, K. S. 1974, ApJ, 191, 499
Palenzuela, C., Lehner, L., & Yoshida, S. 2010, PhRvD, 81, 084007
Papaloizou, J., & Lin, D. N. C. 1984, ApJ, 285, 818
Papaloizou, J. C. B., & Lin, D. N. C. 1995, ARA&A, 33, 505
Pringle, J. E. 1991, MNRAS, 248, 754
Rafikov, R. R. 2016, ApJ, 831, 122
Roedig, C., Krolik, J. H., & Miller, M. C. 2014, ApJ, 785, 115
Roedig, C., Sesana, A., Dotti, M., et al. 2012, A&A, 545, A127
Ryan, G., & MacFadyen, A. 2017, ApJ, 835, 199
Savonije, G. J., Papaloizou, J. C. B., & Lin, D. N. C. 1994, MNRAS, 268, 13
Shi, J.-M., Krolik, J. H., Lubow, S. H., & Hawley, J. F. 2012, ApJ, 749, 118
Shiokawa, H., Cheng, R. M., Noble, S. C., & Krolik, J. H. 2017, ApJ, submitted (arXiv:1701.05610)
Tang, Y., Haiman, Z., & MacFadyen, A. 2018, MNRAS, submitted (arXiv:1801.02266)
Tang, Y., MacFadyen, A., & Haiman, Z. 2017, MNRAS, 469, 4258
Tóth, G. 2000, JCoPh, 161, 605
Zilhão, M., & Noble, S. C. 2014, CQGra, 31, 065013
Zurek, W. H., & Benz, W. 1986, ApJ, 308, 123